Environmental Science Nano

Photochemistry of Ferritin Decorated with Plasmonic Gold Nanoparticles

Journal:	*Environmental Science: Nano*
Manuscript ID	EN-ART-09-2018-001000.R2
Article Type:	Paper
Date Submitted by the Author:	21-Nov-2018
Complete List of Authors:	Cerkez, Elizabeth; Temple University, Chemistry Dutton, Kaitlyn; Temple University, Chemistry Ghidey, Yonatan; Temple University, Chemistry Kukulka, Mark; Temple University, Chemistry Valentine, Ann; Temple University, Department of Chemistry Strongin, Daniel; Temple University, Chemistry; Temple University,

Environmental Significance

The idea of using solar radiation to drive environmental remediation is appealing, but many current catalysts can use only the high energy ultraviolet portion of the solar spectrum. Developing remediation catalysts that can harness the visible region of the spectrum might lead to a more practical process. In this work we demonstrate that the coupling of a plasmonic gold nanoparticle to an established bio-photocatalyst, ferritin, results in a heterostructure that can efficiently reduce hexavalent chromium, a known carcinogen, with visible light.

Photochemistry of Ferritin Decorated with Plasmonic Gold Nanoparticles

Elizabeth B. Cerkez, Kaitlyn G. Dutton, Yonatan G. Ghidey, Mark A. Kukulka, Ann M. Valentine, and Daniel R. Strongin[*]

Department of Chemistry, Temple University, Philadelphia, PA 19122

[*]To whom correspondence should be addressed; dstrongi@temple.edu

Abstract

The photochemistry of a plasmonic biomaterial that consisted of gold nanoparticles (AuNP) on the exterior of the iron sequestration protein, ferritin (Ftn), was investigated. The light driven photochemistry of the hybrid system was studied mechanistically and for the reduction of the high priority pollutant, chromate, Cr(VI) as CrO_4^{2-}. In the absence of aqueous Cr(VI), but in the presence of a sacrificial electron donor, the Fe(III) oxyhydroxide semiconducting core of Ftn underwent a photoreaction to release Fe(II) when exposed to light having wavelengths, $\lambda < 475$ nm. AuNP grown on the exterior of the Ftn produced plasmonic heterostructures (Au/Ftn) that allowed similar photochemistry to occur at longer wavelengths of light (i.e., $\lambda > 475$ nm). Au/Ftn also facilitated the reduction of Cr(VI) to Cr(III) in the presence of visible light ($\lambda > 475$ nm), a reaction that was not observed if AuNP were not attached to the Ftn cage. Results also indicated that AuNP need to be intimately bound to Ftn to extend the photochemistry of Au/Ftn to longer light wavelengths, relative to Au-free Ftn.

1.0 Introduction

In the context of applications for environmental chemistry, desirable properties for heterogeneous semiconducting photocatalysts include colloidal stability, chemical stability towards photocorrosion, and a band gap that can be accessed by large swaths of the solar spectrum.[1] Many traditional metal oxide photocatalysts, including titanium oxide, zinc oxide, and iron oxide, however lack at least one of these preferred properties. For example, while titanium oxide shows excellent structural stability under a range of conditions, it lacks a bandgap that can be excited in the visible light region and thus it is primarily active under ultraviolet (UV) irradiation, which makes up less than 10 % of the solar spectrum. In contrast, iron oxides, which have a more accessible band gap, just within the high energy side of the visible light spectral region, are susceptible to photocorrosion. Designing and realizing photocatalysts that are structurally stable during excitation by visible light would be beneficial for many environmental applications.

While an unconventional photocatalytic system, the iron sequestration protein, ferritin (Ftn), has been shown in prior studies to exhibit properties that could make it a potentially useful photocatalyst. Ferritin is a 24-subunit cage-like protein (Figure 1A), with a biological function to sequester and store iron by catalytically oxidizing toxic ferrous species to a ferric-containing ferrihydrite (Fh) phase stored within the cage.[2-4] The mammalian protein occurs with variable compositions of an H-chain subunit, which has a ferroxidase center to catalyze ferrous oxidation, and an L-chain subunit, which lacks this enzymatic site. The spherical cage has a 12 nm outer diameter and an 8 nm inner diameter and can hold up to ~4500 Fe atoms.[2-4] Previous research from our laboratory demonstrated that the exposure of Ftn to Cr(VI) and light with wavelength, $\lambda \leq 475$ nm resulted in the reduction of Cr(VI) to Cr(III) due to the photoexcitation of the

semiconducting Fh core.[3, 5] Additional research showed that Ftn can photocatalytically reduce a wide range of compounds including polyoxometalate (POM), cytochrome c, and gold salts.[6, 7] A significant benefit of Ftn is that the hydrophilic nature of the protein cage exterior maintains the encapsulated Fh as a colloidal suspension. Additionally, because of the protein function, photocorrosion processes of the iron oxyhydroxide core would be expected to be suppressed by Ftn. The photocorrosion process[8] for the iron oxides results from the photoexcitation of the oxide bandgap (in the presence of an electron donor), leading to the formation of soluble Fe(II) product. In oxic solutions, the released Fe(II) is susceptible to oxidation by dissolved O_2 which leads to reprecipitation of Fe(III)-bearing oxide and results in a non-colloidal solution in the presence of light. Prior studies show that Ftn limits this process, since Ftn sequesters aqueous Fe(II) and oxidizes it to Fe(III) in the interior of the protein cage, regenerating the Fh core.[3, 5]

While Ftn is a potentially attractive colloidal photocatalyst, decreasing the photochemical energy requirement (defined by the band gap of the Fh core) to absorb a wider range of solar radiation would be advantageous. Sensitizing semiconductor photocatalysts so that they can be excited by light having energies less than the bandgap has seen substantial research efforts. Many of these prior studies have been focused on synthesizing heterostructures with a visible light active sensitizer.[9, 10] With regard to sensitizers, metal nanoparticles offer superior chemical stability compared to organic dyes (used in photovoltaic cells) and can similarly be excited by the absorption of visible light, due to the presence of a surface plasmon resonance (SPR).[11] Excitation of a metallic nanoparticle SPR which is chemically bound directly to the semiconductor (or to a thin interfacial layer of a third material) can lead to electron population in the conduction band of the host material via multiple pathways depending on the particular organization of the heterostructure components. Such studies have often investigated

semiconductors, such as titanium oxide and iron oxide, bound to plasmonic particles (such as Au nanoparticles (AuNP)), though a motivation exists to find more earth-abundant metal plasmonic materials.[11-13] Relevant to the aims of the present study, this earlier work has investigated the application of hybrid iron oxide-plasmonic gold structures for various photocatalytic applications, which have included the degradation of dyes and water splitting. [14-17]

The hypothesis tested in this study is that the attachment of a Au plasmonic nanoparticle, having a SPR in the visible region (~532 nm), to Ftn will allow the photochemistry of Au/Ftn (and its iron oxide core) to be extended to longer wavelengths of light (e.g., extended to $\lambda \geq 475$ nm). To test this hypothesis, AuNP were grown on the exterior of the protein cage of Ftn (Au/Ftn), and the photochemistry of Au/Ftn was compared to Au-free Ftn in the context of Fe(II) release and for the reduction of chromate during light excitation. To address the sensitization of Ftn by AuNP, a major research focus was to compare the light wavelength dependence of these photochemical reactions in the presence of Au/Ftn and Ftn. Results will suggest that the Au/Ftn system exhibits properties associated with a potentially viable photocatalyst (sensitized, colloidal, and stable) and that the plasmonic biomaterial has potential relevance to environmental remediation, specifically in regards to the reduction of the high priority pollutant, chromate.

2.0 Experimental

2.1 Materials: Horse spleen apoFtn (~85-90% L chain without an Fe bearing core) was sourced from Calzyme, ferrozine from ACROS Organics, and all other reagents from Sigma Aldrich and Fisher Scientific. All materials were of analytical grade. Deionized (DI) water (18 MΩ cm^{-1}) was used to prepare all solutions.

2.2 Synthesis of Protein Samples: The preparation of iron loaded Ftn was adapted from Kim et al.[5] ApoFtn, 10 mg, was dissolved in 40 mL of 0.10 M NaCl (pH 7.4). To the ApoFtn solution, a total of 1.0 mL of anoxic $Fe(NH_4)_2(SO_4)_2 \cdot 6H_2O$ (10 mg/mL) was added in four equal aliquots (0.25 mL) every hour. Ftn-Fe(II) solutions were allowed to air-oxidize overnight at 4 °C. The Ftn was then dialyzed against Tris buffer (0.1 M, pH 7.4) for 48 hours and stored at 4 °C.

A photochemical synthesis was used to grow AuNPs on the Ftn cage. The synthetic protocol was adapted from Keyes et al.[18] and Petrucci et al.[19] Briefly, the reaction solution containing 0.34 μM Ftn, 50 mM NaCl, 30 mM sodium citrate, 20 mM Tris (pH 7.4), and 0.4 mM $HAuCl_4$ was added to a 1 cm^2 quartz cuvette (total volume of 3.1 mL). The cuvette was then exposed to simulated solar radiation (SSR) for 6 minutes from the output of a 900 W high-pressure Xenon lamp (Schoeffel Instruments, Westwood, NJ). Ultraviolet visible spectroscopy (UV-Vis) was carried out (Evolution 901 spectrometer (Thermo Sci)) after each synthesis batch to confirm the presence of AuNP via the appearance of the surface plasmon resonance at ~530-540 nm. The synthesis was followed by dialysis against Tris buffer (0.1 M, pH 7.4).

During the course of photochemical AuNP synthesis, a Fe(II) photoproduct was expelled from the protein. To replace this iron that left the protein, portions of Au/Ftn were exposed a second time to anoxic $Fe(NH_4)_2(SO_4)_2 \cdot 6H_2O$ (10 mg/mL). The volume of the Fe(II)-solution used depended on the desired Fe loading, and the resulting solution was exposed to air overnight. No precipitation or aggregation was observed during this reloading process, suggesting that the AuNP on the exterior of the protein did not affect the Fe-loading process. Au/Ftn samples were then dialyzed against Tris buffer (0.1 M, pH 7.4).

AuNPs in the absence of Ftn were synthesized via an adapted heated synthesis,[20] where sodium citrate (35 mM) was heated to 95 ºC after which $HAuCl_4$ (25 mM) was added. The

solution changed from yellow to colorless to black, as Au(III) was reduced to Au(0). In less than 60 s the solution turned red/purple, characteristic of AuNP in solution. The solution was then centrifuged and rinsed with DI H_2O, to remove excess citrate. We note that attempts to exchange/remove all citrate from solution, via dialysis against Tris, resulted in immediate visible aggregation and loss of colloidal stability.

2.3 Heterostructure Characterization: Inductively coupled plasma - optical emission spectroscopy (ICP-OES) was used to quantify the iron and gold concentrations associated with Au/Ftn and Ftn samples. A Thermo-Scientific iCAP 7400-ASX520 was used for the quantification. Samples for analysis were diluted to 5 mL and acidified 2% by volume with HNO_3. Iron data were collected in axial mode at 259.940 nm and gold data were collected in axial mode at 242.795 nm. Transmission electron microscopy (TEM) was used to image Ftn and Au/Ftn using either a JEOL JEM-1400 TEM operating at 120 kV or a JEOL JEM-3010 TEM operating at 300 kV. Samples were prepared on holey carbon TEM grids (Ted Pella) and allowed to dry as a thin film. Some samples were negatively stained with a 2% phosphotungstic acid (PTA) solution at pH 7 prior to imaging, to allow imaging of the protein shell of Ftn (see Supporting Information, Figure S1).

2.4 Photochemical Batch Reactions: All photochemical experiments had a reaction volume of 3.1 mL and were carried out in a 1 cm^2 quartz cuvette using the same xenon lamp described above. Additionally, all photochemical experiments were carried out in duplicate, displayed by error bars on plots. Absorbance spectra associated with time 0 were collected before exposure to the SSR source. Samples were illuminated for a total of 45 min, unless otherwise noted, and at each time point the cuvette was removed from illumination and a UV-Vis scan was taken of the sample from 700-200 nm. The light wavelength dependence of the photochemical reactions was

determined using longpass wavelength cutoff filters; 475, 570, and 625 nm optical glass filters (Schott).

Photochemical batch reactions were conducted in the presence of ferrozine or Cr(VI) depending on the specified conditions. Experiments that monitored Fe(II) release contained the following reaction conditions: 0.035 μM Ftn, 32 mM sodium tartrate, and 0.714 mM ferrozine in 60 mM Tris buffer (pH 7.4) at a total volume of 3.1 mL. Experiments that monitored Cr(VI) reduction used the above conditions, but replaced ferrozine with 0.200 mM Cr(VI) ($K_2Cr_2O_7$). Volume changes were compensated for by adjusting the volume of Tris buffer. Separate calibration curves for ferrozine-Fe(II) (λ_{max} 562 nm) and Cr(VI) (λ_{max} 372 nm) were completed in Tris buffer and used to quantify reaction concentrations.

Monochromatic photoexcitation experiments were conducted in a 1 cm^2 quartz cuvette with the same reaction conditions described above but were exposed to 532 nm light from a CW laser source (Opus, Laser Quantum). Two dielectric mirrors (>99% reflectivity) were used to direct the unfocused (collimated) laser beam into the cuvette. The light intensity can be calculated using the relation:

$$I = \frac{P}{\pi(0.1)^2} \approx \frac{P}{0.031416}$$

where I is intensity in watts per square centimeter (W/cm^2), P is power in watts (W), and 0.1 cm is the beam radius. For example, at a laser power of 0.45 W the intensity will be ~14.3 W/cm^2. The home-built UV-Vis spectrometer is based on the design of Kirchner et al.[21] The output of a fiber-coupled deuterium-tungsten lamp (DH-2000-BAL, Ocean Optics) was collimated and refocused into the cuvette using parabolic mirrors, and the transmitted light was fiber-coupled to a USB spectrometer (HR4000, Ocean Optics) in the same manner.

3. Results and Discussion

TEM of the Au/Ftn showed that the diameter of the AuNP on the exterior of the Ftn protein cage were 7.6 ± 1.7 nm (SI, Figure S2 and S3). Previous research suggested that the AuNP formation occurred on cysteine groups located on the three fold channels of Ftn, indicated by yellow residues in Figure 1A, due to the thiophilicity of gold. We note that research has also utilized the affinity of cysteine for Au to link Au plasmonic particles to iron oxide (protein free systems) in the synthesis of hybrid photocatalysts.[14] TEM imaging of the heterostructures synthesized in our laboratory after a negative stain was applied (Figure 1B) exhibits structures that show gold nanoparticles (dark spheres) associated with Ftn protein cages (light gray spheres), consistent with the previously published studies.[18, 19] We note that all images display some single particle structures, i.e., unattached protein cages and unattached gold nanoparticles. Based on an image analysis of 1000 individual Ftn cages, ~86% of the Ftn cages are attached to a gold nanoparticle. We do hold out the possibility that some of what are called unattached AuNP could be attached to Ftn, but obscuring the protein if it is immediately above or below the Au. In short, it is possible that >86% of the Ftn is attached to AuNP. The stability of the colloid solution is consistent with the vast majority of the AuNP being attached to protein cages. UV-vis spectroscopy of the Au/Ftn system exhibits an SPR with an absorption maximum at ~532 nm (SI, Figure S4). The plasmon absorbance of Au/Ftn is broader than the SPR associated with AuNP alone (also shown in Figure S4) which is likely due to the differences in local dielectric environment between free-AuNP and those bound to the ferritin protein.[22] Any detailed comparison of these spectra would be dubious, however, since we cannot rule out that a minority fraction of free AuNP is contributing to the SPR feature in the Au/Ftn spectrum. We prepared Ftn and Au/Ftn biomaterials with a variety of Fe-loadings, and refer to the samples used as

Ftn(1200), Au/Ftn(800), Au/Ftn(1200), and Au/Ftn(2000), where the values in parentheses are the average number of Fe atoms mineralized in an individual protein cage. These loadings were determined by assuming average distributions of the available Fe (determined by ICP-OES) across the total number of protein cages available (SI, Figure S5).

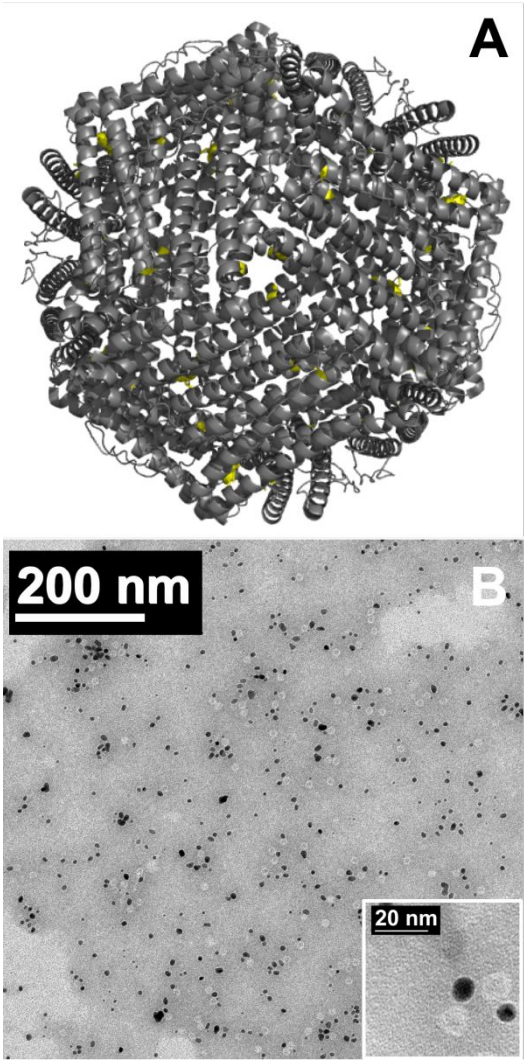

Figure 1 – (A) Structure of horse spleen ferritin (PDB ID 2W0O)[23] with cysteine residues labeled in yellow. (B) TEM of Au/Ftn(2000) heterostructures where dark spheres are AuNP and light spheres are protein cages. At least 86% of the Ftn are in direct contact with AuNP. Inset shows a higher magnification TEM image of Au/Ftn heterostructures.

The effect of the Au SPR on the excitation of the inorganic iron oxyhydroxide core of Ftn was investigated by measuring the release of Fe(II) during exposure to light. Photochemical experiments to investigate Fe(II) release were conducted by individually mixing Ftn and Au/Ftn with a hole scavenger (i.e., sodium tartrate), ferrozine, and buffer (Tris, pH 7.4). These solutions were then exposed to SSR or to filtered light of specific wavelength ranges using optical longpass filters. Ferrozine[24] was used to chelate the aqueous Fe(II) exiting the protein during photoexcitation and the concentration of the ferrozine-Fe(II) complex was quantified by UV-vis spectroscopy as a function of exposure time. Analysis of these data allowed the rate of Fe(II) release to be determined for a given solution, either pure Ftn, Au/Ftn, or AuNP-Ftn mixtures.[7] We note that soluble Fe(II) was not detected if ferrozine was added after irradiation due to the rapid reentry and re-mineralization of Fe(II) in the Ftn interior. Control studies indicated that the ferrozine-Fe(II) complex was both stable under irradiation and that the presence of ferrozine did not induce Fe(II) release from the proteins in the absence of light (see SI, Figures S6 and S7).

Exposure of Ftn(1200), Au/Ftn(800), Au/Ftn(1200), and Au/Ftn(2000) to SSR resulted in Fe(II) release from all protein systems, determined by the growth of an absorbance at 562 nm (ferrozine-Fe(II) complex) by UV-vis spectroscopy (see SI, Figure S8). The Fe(II) released from the four different samples as a function of time is shown in Figure 2A. At least two important experimental observations can be used to distinguish the photochemistry between Au/Ftn and Ftn: (1) the rate at which Fe(II) was released and (2) the total amount of Fe(II) released over the time of light exposure (Table 1). We take special note of Ftn(1200) and Au/Ftn(1200), which have the same initial Fe loading, but display a significant difference in the rate of Fe(II) release. An analysis of the average initial rate of release over the first 5 min of irradiation for equimolar protein solutions shows that Au/Ftn(1200) releases Fe(II) four times faster than Ftn(1200). This

dramatic increase in Fe(II) release rate when Au is attached to a majority of the protein cages is also apparent in heterostructures with Fe loadings higher and lower than 1200, i.e. the Au/Ftn(800) and Au/Ftn(2000) systems. After 25 min of illumination the concentration of Fe(II) released from these Au/Ftn samples into solution reaches a steady state, suggesting that after this exposure time no further Fe(II) leaves the protein shell. In contrast, after 45 min illumination, Ftn still exhibits Fe(II) release, reflective of its slower Fe(II) release rate. Under these illumination conditions, all proteins release greater than 82% of the available Fe mineralized initially in their respective protein cage, and remained colloidal both during and after exposure to SSR.

Table 1. Release of Fe(II), as quantitated by ferrozine complexation, during irradiation[a] of iron-loaded ferritin/gold nanoparticle heterostructures and related materials.

	SSR		λ ≥ 475 nm		λ ≥ 570 nm	
	Initial rate ($M \cdot s^{-1}$)	$[Fe(II)]_{45min}$ (μM)	Initial rate ($M \cdot s^{-1}$)	$[Fe(II)]_{45min}$ (μM)	Initial rate ($M \cdot s^{-1}$)	$[Fe(II)]_{45min}$ (μM)
Ftn(1200)	2.5×10^{-8}	35	1.8×10^{-9}	3.9	-	< 1
Au/Ftn(800)	5.5×10^{-8}	24	1.5×10^{-8}	15	1.1×10^{-9}	1.2
Au/Ftn(1200)	1.1×10^{-7}	38	3.7×10^{-8}	34	1.1×10^{-9}	2.9
Au/Ftn(2000)	1.8×10^{-7}	59	8.9×10^{-8}	52	1.6×10^{-9}	4.9
AuNP + Ftn(1200)	2.8×10^{-8}	34	1.8×10^{-9}	4.4	-	< 1

[a] Irradiation with light λ ≥ 625 nm resulted in $[Fe(II)]_{45min}$ < 1 μM for all samples.

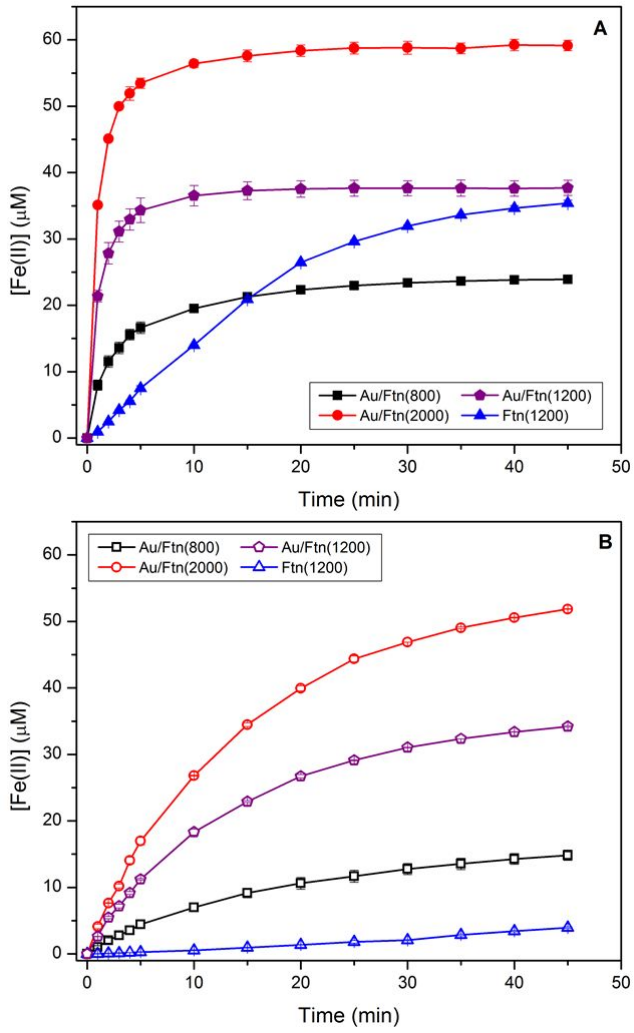

Figure 2 –Ferrous iron release from Au/Ftn and Ftn during exposure to (A) SSR and (B) light wavelengths ≥ 475 nm. (Some error bars smaller than symbols)

To further analyze the effect of Au on the kinetics of Fe(II) release we exposed the different protein samples to broad spectrum radiation with $\lambda \geq 475$ nm (i.e., $h\nu \leq 2.6$ eV), $\lambda \geq 570$ nm, and $\lambda \geq 625$ nm. Using these wavelength ranges (relative to un-filtered light) we could selectively reduce the number of photons which could excite the bandgap of the Fh core directly ($\lambda \geq 475$ nm) or both the Fh core and portions of the Au SPR ($\lambda \geq 570$ nm and $\lambda \geq 625$ nm). Exposure of Ftn and Au/Ftn to the wavelength range of $\lambda \geq 475$ nm, resulted in an overall decrease in the amount of Fe(II) release from all protein samples, compared to exposing the same respective samples to SSR (Figure 2B). For example, after Ftn(1200) was exposed to $\lambda \geq 475$ nm for 45 min, the total concentration of iron release was 3.9 μM, compared to a value of 35.4 μM when the sample was exposed to SSR (i.e., an 89% decrease in Fe(II) release). The substantial decrease in Fe(II) release is consistent with the bandgap of the Fh core having a value of ~2.6 eV.[25, 26] In contrast to Ftn(1200), the Au containing heterostructures exhibited a much smaller decrease in the amount of Fe(II) release compared to SSR (Table 1). After a 45 min exposure of Au/Ftn(800), Au/Ftn(1200), and Au/Ftn(2000) to light with $\lambda \geq 475$, the Fe(II) concentrations in solution were 14.8, 34.2, and 51.9 μM, respectively. The initial average rate of ferrous iron release from equimolar protein solutions over the first 5 min from Au/Ftn(1200) was 20 times greater than the release rate from Ftn(1200) showing that the Au-induced photo-sensitization effect is significant.

Exposure of Ftn(1200) to light with $\lambda \geq 570$ nm resulted in less than 1 μM Fe(II) in solution (see SI, Figure S9). Heterostructures containing Au, Au/Ftn(800), Au/Ftn(1200), and Au/Ftn(2000), however, released 1.2, 2.9, and 4.9 μM, respectively, representing approximately ~8-9% of the amount of Fe(II) released when $\lambda \geq 475$ nm light was used. This observed Fe(II) release for the Au/Ftn systems can be attributed to the excitation of a portion of the SPR just

above (i.e., longer wavelength side) the absorption maximum (532 nm). Finally, exposing the heterostructures to wavelengths of light that could not effectively excite the SPR ($\lambda \geq 625$ nm) resulted in the release of less than 1 μM Fe(II) for all samples studied (see SI, Figure S10). Overall, these experimental results indicate that the presence of AuNP bound to Ftn allows longer wavelength light to be used to activate the protein for Fe(II) release, relative to Ftn alone.

In addition to kinetic analysis under polychromatic illumination, we exposed Ftn(1200) and Au/Ftn(1200) to monochromatic laser-light (λ=532 nm) aligned with the Au SPR maximum. When Ftn(1200) was illuminated with this monochromatic radiation for 10 min we observed no release of Fe(II) (Figure 3A). In contrast, exposure of Au/Ftn(1200) to 532 nm light showed a release of Fe(II) from the heterostructure, indicated by the growth of a shoulder centered at 562 nm (absorbance of ferrozine-Fe(II) complex – Figure 3A inset). This experimental observation of Fe(II) release from Au/Ftn(1200) during exposure to only 532 nm light strongly suggests that excitation of the SPR results in the electron population of the conduction band of the iron oxide core of Ftn. The result of this conduction band population is the reduction of Fe(III) to Fe(II) and the concomitant release of this reduction product into solution. We note that Fe(II) release is significantly less than that observed from the experiments with longpass filters. Under monochromatic light excitation, the illumination beam is significantly smaller than the broad spectrum beam and more importantly, only the absorption maximum of the SPR is excited.

To further analyze the effect of the Au SPR we tested whether direct contact between AuNP and Ftn was needed for an enhancement in photochemistry. Experiments were performed that quantified Fe(II) release during the irradiation of a co-mixture of Ftn and AuNP (AuNP + Ftn). Using a thermal method described in the literature, AuNP were synthesized, characterized (see SI, Figure S11), and then mixed with Ftn(1200), resulting in a heterogeneous mixture,

instead of a heterostructure.[20] AuNP prepared in this way exhibited a similar SPR absorption maximum as AuNP bound to Ftn (see SI, Figure S4). The AuNP concentration in these experiments was equivalent to the amount of Au present in the photochemical experiments using Au/Ftn that were discussed above. Illumination of the mixture of AuNP and Ftn (Figure 3B) resulted in an average initial rate of Fe(II) release of 2.8×10^{-8} M s^{-1}, similar to when a Au-free Ftn solution was exposed to light under the same conditions (2.5×10^{-8} M s^{-1}). Exposure of the AuNP + Ftn mixture to visible light ($\lambda \geq 475$ nm) resulted in < 5 μM of Fe(II), consistent with Fe(II) release within a Au-free Ftn solution (dashed overlay reproduced from Figure 2B). Furthermore, exposure of the AuNP + Ftn to monochromatic laser light (532 nm) resulted in no release of Fe(II) (see SI, Figure S12). These experimental results indicate that excitation of the Au SPR of non-associated nanoparticles had no effect on the Fe(II) release rate from Ftn. Thus, intimate contact between AuNP and Ftn is a pre-requisite for Au to enhance Fe(II) release from Ftn during exposure to long wavelength radiation. This result also suggests that any free AuNP co-existing with Au/Ftn would not be expected to play any role in the Au/Ftn photochemistry.

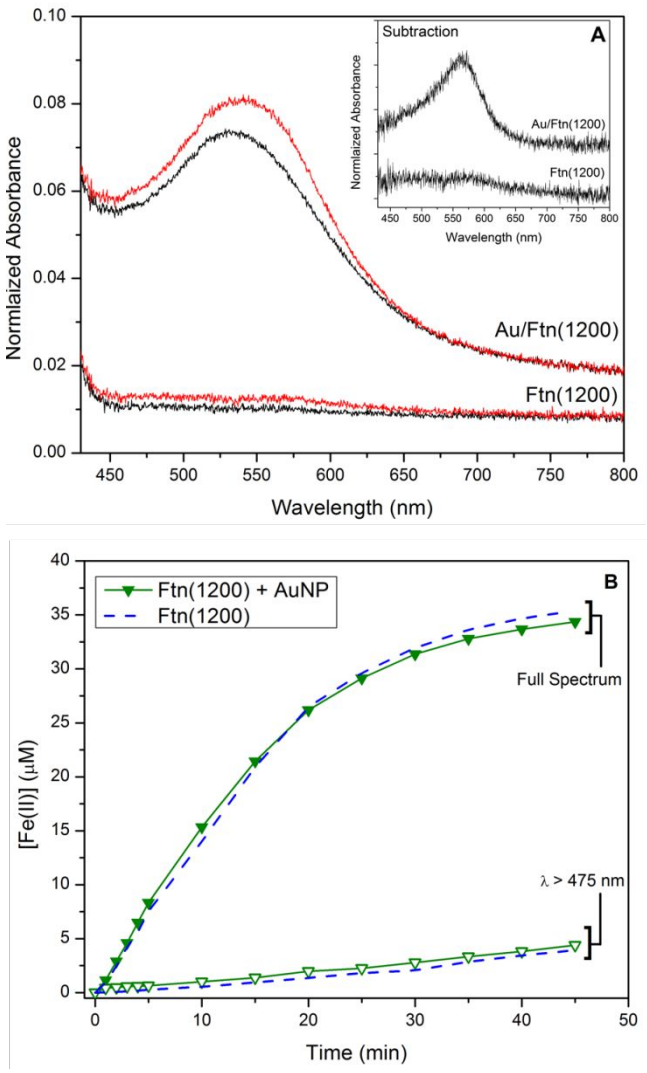

Figure 3 – UV-vis spectra of (A) Ftn and Au/Ftn before and after exposure to monochromatic (532 nm) light. The inset displays difference spectra derived from before and after exposure data. The difference spectrum for Au/Ftn isolates the absorbance due to the Fe(II)-ferrozine complex from the plasmon resonance absorption of the AuNP on the Ftn. (B) Release of Fe(II) from heterogeneous mixture of AuNP and Ftn upon exposure to SSR and light $\lambda \geq 475$ nm.(Ftn(1200) traces replicated from Figure 2A and 2B)

The utility and light wavelength dependence of Au/Ftn as a photocatalyst for the conversion of the high priority pollutant, chromate (Cr(VI)), to trivalent chromium (Cr(III)) were also investigated.[5] Prior research from our laboratory showed that this redox chemistry can be facilitated by Ftn when illuminated with light having a $\lambda < \sim 475$ nm.[5] The exposure of Ftn(1200) and Au/Ftn(1200) to 200 μM of Cr(VI), and irradiated with SSR, resulted in a 100 % conversion of Cr(VI) to Cr(III) in all cases within 25 min of exposure time (Figure 4A). In contrast, experiments where Ftn(1200) and Cr(VI) were exposed to light with $\lambda \geq 475$ nm resulted in an insignificant amount of Cr(VI) reduction (Figure 4B), but the exposure of Au/Ftn(1200) and Cr(VI) resulted in the reduction of ~85 μM of Cr(VI). During the photo-exposure studies, the Au/Ftn systems remained colloidal both during and after exposure to radiation, similar to the non-Au counterparts. Control experiments were also conducted where AuNP alone in solution were exposed to Cr(VI). In neither scenario (exposure to SSR or $\lambda \geq 475$ light) was appreciable Cr(VI) reduction observed (Figure 4A and 4B) indicating that AuNP alone were not active for this photochemistry.

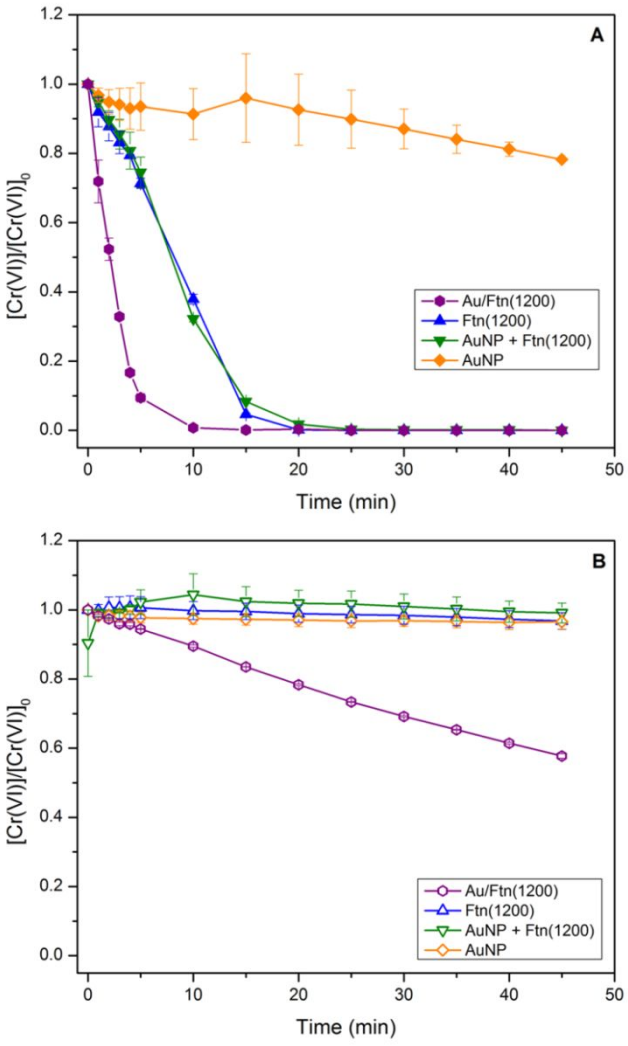

Figure 4 – Reduction of Cr(VI) in the presence of different Ftn and AuNP systems resulting from exposure to (A) SSR and (B) light wavelengths > 475 nm.

The reduction of Cr(VI) by Fe(II) is well studied and should occur in a 1:3 stoichiometry;[27] however in these experiments too little Fe(II) leaves the protein cage (max of 67 μM from Au/Ftn(2000)) to account for the reduction of 200 μM Cr(VI) that is experimentally observed during exposure to broad spectrum light. The presence of tartrate in solution, utilized as a hole scavenger, is also known to be a UV light-activated reducing agent of Cr(VI) and can reduce between 30-100% of Cr(VI) present, depending on the absence or presence of Fe,

respectively (see SI, Figure S13).[28-30] The reduction by UV-activated tartrate however is not a viable mechanism to explain the amount of Cr(VI) reduction in the case of exposure to $\lambda \geq 475$ nm light, since less than 6% of Cr(VI) is reduced by a tartrate-Fe(II) only mechanism under these conditions (see SI, Figure S13). In particular, Au/Ftn(1200) releases 34.2 μM Fe(II) after 45 minutes exposure to $\lambda \geq 475$ nm but we observe ~85 μM of Cr(VI) reduced for the same exposure time; approximately 7.5 times more Cr(VI) reduced than should be observed via a homogenous reaction with Fe(II). While nonstoichiometric, the percent of Cr(VI) reduced does correlate with the iron oxide core size, since Au/Ftn(2000) can reduce more Cr(VI) than Au/Ftn(1200) which can reduce more than Au/Ftn(800) (see SI, Figure S14). Thus, the size of the iron oxide core of Ftn is a factor in how much Cr(VI) is reduced. Another factor which could explain the extra-stoichiometric reduction is the potential for electron transfer directly through the protein shell.[31] Previous work has demonstrated that horse spleen Ftn is conductive, and hence the excited electrons in the conduction band of the iron oxide core, generated by AuNP excitation, may be accessible to Cr(VI) directly through the protein. Further, the photoreduction of Cr(VI) by iron oxide minerals has been previously supposed to occur via a catalytic mechanism, where Cr(III) is produced by a heterogeneous reduction, versus a homogeneous reduction with Fe(II).[32] This phenomenon is likely due to the reduction potential of Cr(VI) (-5.83 eV) lying below the conduction band minimum of most iron oxide minerals, which would be similarly true of the Fh core in Ftn (-5.08 eV). Reduction of Cr(VI) directly via electron transfer through the protein shell could explain the dependence of percent Cr(VI) reduced on Fe core size. A larger Fh core might be expected to have more contact points with the interior of the protein cage, thus making electron transfer more efficient. Lastly, we also note that all of the photochemical studies demonstrate that a hole scavenger must be present in solution to

compensate for holes produced in the valence band of the mineral core, a process that likely would also occur via charge transfer through the protein shell.

With regard to the mechanism by which the Au SPR alters the photochemistry of Ftn, at least two possible mechanisms might be considered that have been previously proposed for semiconductor – SPR particle systems;[33] direct electron transfer (DET) and resonant energy transfer (RET). The process for DET would involve the excitation of the SPR and an excited "hot" electron being transferred to the conduction band of the semiconductor, where a prerequisite is direct contact between the plasmonic metal and semiconductor.[13] While TEM of heterostructures suggests that the Fh semiconductor and AuNP are physically separated by the protein shell, as stated above previous work has shown that the ferritin protein exhibits electrical conductivity, and hence a DET type process could possibly occur.[31, 34, 35] In contrast, RET is due to the relaxation of the excited plasmon states, which through dipole coupling results in the formation of a hole and excited electron in the nearby semiconductor.[15] Prior studies have shown that this mechanism is operative when a semiconductor and a plasmonic material are physically separated from each other with a nonconductive SiO_2 barrier (< 10 nm).[33] Thus for the Au/Ftn heterostructure, the presence of the 2 nm protein shell between the gold nanoparticle and semiconductor core of Ftn would likely not suppress the RET process. Whether DET and/or RET is the operative mechanism for Au/Ftn is not ascertainable with the current study. Experiments ongoing in our laboratory, however, are being designed to determine the relative contribution of each mechanism during Au/Ftn photochemistry.

4.0 Conclusions

Results presented here show that AuNPs directly bound to the exterior of Ftn extend the photochemistry of Au/Ftn to longer light wavelengths compared to Ftn alone. In the context of environmental remediation strategies, the ability for Au/Ftn to access more of the solar spectrum improves upon the already desirable qualities of colloidal and catalytic stability that are properties of Ftn. Experiments are currently being designed to elucidate the sensitization mechanism to better engineer the novel hybrid photocatalyst. Further, the results indicate that under visible light conditions the Au/Ftn system reduces more of the high priority pollutant, chromate, than would be possible with a homogenous system. Thus the Au/Ftn system should be further explored for facilitating other environmentally relevant heterogeneous redox chemistry. With recognition of the cost and availability of gold, future work will also focus on synthesizing other possible plasmonic biomaterials with a focus on non-noble metal based systems, such as nickel, copper, and aluminum.

5.0 Conflicts of Interest

There are no conflicts to declare.

6.0 Acknowledgements

We thank Johanan Odhner for equipment and help on the monochromatic light experiments. We thank Farbod Alimohammadi and Dr. Ke Chen for help in acquiring the TEM images and acknowledge the use of services and facilities of the Temple Materials Institute at Temple University. K.G.D. thanks the Temple Francis Velay Fellowship for summer support. A.M.V. thanks the National Science Foundation (CHE-1412373 and CHE-1708793) for support.

7.0 References:

1. D. Chen, M. Sivakumar and A. K. Ray, Heterogeneous Photocatalysis in Environmental Remediation, *Developments in Chemical Engineering and Mineral Processing*, 2000, **8**, 505-550.
2. E. C. Theil, R. K. Behera and T. Tosha, Ferritins for chemistry and for life, *Coordination Chemistry Reviews*, 2013, **257**, 579-586.
3. F. M. Michel, H.-A. Hosein, D. B. Hausner, S. Debnath, J. B. Parise and D. R. Strongin, Reactivity of ferritin and the structure of ferritin-derived ferrihydrite, *Biochimica et Biophysica Acta (BBA) - General Subjects*, 2010, **1800**, 871-885.
4. P. Arosio, L. Elia and M. Poli, Ferritin, cellular iron storage and regulation, *IUBMB Life*, 2017, **69**, 414-422.
5. I. Kim, H.-A. Hosein, D. R. Strongin and T. Douglas, Photochemical Reactivity of Ferritin for Cr(VI) Reduction, *Chemistry of Materials*, 2002, **14**, 4874-4879.
6. V. V. Nikandrov, C. K. Grätzel, J. E. Moser and M. Grätzel, Light induced redox reactions involving mammalian ferritin as photocatalyst, *Journal of Photochemistry and Photobiology B: Biology*, 1997, **41**, 83-89.
7. N. Saenz, M. Sánchez, N. Gálvez, F. Carmona, P. Arosio and J. M. Dominguez-Vera, Insights on the (Auto)Photocatalysis of Ferritin, *Inorganic Chemistry*, 2016, **55**, 6047-6050.
8. N. Bhandari, R. J. Reeder and D. R. Strongin, Photoinduced Oxidation of Arsenite to Arsenate on Ferrihydrite, *Environmental Science & Technology*, 2011, **45**, 2783-2789.
9. J. Cai, X. Wu, S. Li and F. Zheng, Controllable location of Au nanoparticles as cocatalyst onto TiO_2@CeO_2 nanocomposite hollow spheres for enhancing photocatalytic activity, *Applied Catalysis B: Environmental*, 2017, **201**, 12-21.
10. P. Chowdhury, J. Moreira, H. Gomaa and A. K. Ray, Visible-Solar-Light-Driven Photocatalytic Degradation of Phenol with Dye-Sensitized TiO_2: Parametric and Kinetic Study, *Industrial & Engineering Chemistry Research*, 2012, **51**, 4523-4532.
11. Y. Tian and T. Tatsuma, Plasmon-induced photoelectrochemistry at metal nanoparticles supported on nanoporous TiO_2, *Chemical Communications*, 2004, 1810-1811.
12. E. Kowalska, O. O. P. Mahaney, R. Abe and B. Ohtani, Visible-light-induced photocatalysis through surface plasmon excitation of gold on titania surfaces, *Physical Chemistry Chemical Physics*, 2010, **12**, 2344-2355.
13. C. Clavero, Plasmon-induced hot-electron generation at nanoparticle/metal-oxide interfaces for photovoltaic and photocatalytic devices, *Nat Photon*, 2014, **8**, 95-103.
14. S.-W. Cao, J. Fang, M. M. Shahjamali, Z. Wang, Z. Yin, Y. Yang, F. Y. C. Boey, J. Barber, S. C. J. Loo and C. Xue, In situ growth of Au nanoparticles on Fe_2O_3 nanocrystals for catalytic applications, *CrystEngComm*, 2012, **14**, 7229-7235.
15. J. Li, S. K. Cushing, D. Chu, P. Zheng, J. Bright, C. Castle, A. Manivannan and N. Wu, Distinguishing surface effects of gold nanoparticles from plasmonic effect on photoelectrochemical water splitting by hematite, *Journal of Materials Research*, 2016, **31**, 1608-1615.
16. K. Korobchevskaya, C. George, L. Manna and A. Comin, Effect of Morphology on Ultrafast Carrier Dynamics in Asymmetric Gold–Iron Oxide Plasmonic Heterodimers, *The Journal of Physical Chemistry C*, 2012, **116**, 26924-26928.

17. Y. Li, J. Zhao, W. You, D. Cheng and W. Ni, Gold nanorod@iron oxide core–shell heterostructures: synthesis, characterization, and photocatalytic performance, *Nanoscale*, 2017, **9**, 3925-3933.
18. J. D. Keyes, R. J. Hilton, J. Farrer and R. K. Watt, Ferritin as a photocatalyst and scaffold for gold nanoparticle synthesis, *Journal of Nanoparticle Research*, 2011, **13**, 2563-2575.
19. O. D. Petrucci, D. C. Buck, J. K. Farrer and R. K. Watt, A ferritin mediated photochemical method to synthesize biocompatible catalytically active gold nanoparticles: size control synthesis for small (~2 nm), medium (~7 nm) or large (~17 nm) nanoparticles, *RSC Advances*, 2014, **4**, 3472-3481.
20. J. Piella, N. G. Bastús and V. Puntes, Size-Controlled Synthesis of Sub-10-nanometer Citrate-Stabilized Gold Nanoparticles and Related Optical Properties, *Chemistry of Materials*, 2016, **28**, 1066-1075.
21. F. O. Kirchner, S. Lahme, E. Riedle and P. Baum, All-reflective UV-VIS-NIR transmission and fluorescence spectrometer for μm-sized samples, *AIP Advances*, 2014, **4**, 077134.
22. S. Eustis and M. A. El-Sayed, Why gold nanoparticles are more precious than pretty gold: Noble metal surface plasmon resonance and its enhancement of the radiative and nonradiative properties of nanocrystals of different shapes, *Chemical Society Reviews*, 2006, **35**, 209-217.
23. N. de Val, J.-P. Declercq, C. K. Lim and R. R. Crichton, Structural analysis of haemin demetallation by L-chain apoferritins, *Journal of Inorganic Biochemistry*, 2012, **112**, 77-84.
24. L. L. Stookey, Ferrozine---a new spectrophotometric reagent for iron, *Anal. Chem.* , 1970, **42**, 779-781.
25. J. S. Colton, S. D. Erickson, T. J. Smith and R. K. Watt, Sensitive detection of surface- and size-dependent direct and indirect band gap transitions in ferritin, *Nanotechnology*, 2014, **52**.
26. T. J. Smith, S. D. Erickson, C. M. Orozco, A. Fluckiger, L. M. Moses, J. S. Colton and R. K. Watt, Tuning the band gap of ferritin nanoparticles by co-depositing iron with halides or oxo-anions, *Journal of Materials Chemistry A*, 2014, **2**, 20782-20788.
27. S. E. Fendorf and G. Li, Kinetics of Chromate Reduction by Ferrous Iron, *Environmental Science & Technology* 1996, **30**, 1614-1617.
28. I. P. Pozdnyakov, A. V. Kolomeets, V. F. Plyusnin, A. A. Melnikov, V. O. Kompanets, S. V. Chekalin, N. Tkachenko and H. Lemmetyinen, Photophysics of Fe(III)–tartrate and Fe(III)–citrate complexes in aqueous solutions, *Chemical Physics Letters*, 2012, **530**, 45-48.
29. L. Wang, C. Zhang, F. Wu and N. Deng, Photoproduction and determination of hydroxyl radicals in aqueous solutions of Fe(III)–tartrate complexes: a quantitative assessment, *Journal of Coordination Chemistry*, 2006, **59**, 803-813.
30. I. J. Buerge and S. J. Hug, Influence of Organic Ligands on Chromium(VI) Reduction by Iron(II), *Environmental Science & Technology*, 1998, **32**, 2092-2099.
31. D. Xu, G. D. Watt, J. N. Harb and R. C. Davis, Electrical Conductivity of Ferritin Proteins by Conductive AFM, *Nano Letters*, 2005, **5**, 571-577.
32. B. Deng and A. T. Stone, Surface-Catalyzed Chromium(VI) Reduction: Reactivity Comparisons of Different Organic Reductants and Different Oxide Surfaces, *Environmental Science & Technology*, 1996, **30**, 2484-2494.

33. S. K. Cushing, J. Li, F. Meng, T. R. Senty, S. Suri, M. Zhi, M. Li, A. D. Bristow and N. Wu, Photocatalytic Activity Enhanced by Plasmonic Resonant Energy Transfer from Metal to Semiconductor, *Journal of the American Chemical Society*, 2012, **134**, 15033-15041.
34. U. Carmona, L. Li, L. Zhang and M. Knez, Ferritin light-chain subunits: key elements for the electron transfer across the protein cage, *Chemical Communications*, 2014, **50**, 15358-15361.
35. F. Marken, D. Patel, C. E. Madden, R. C. Millward and S. Fletcher, The direct electrochemistry of ferritin compared with the direct electrochemistry of nanoparticulate hydrous ferric oxide, *New Journal of Chemistry*, 2002, **26**, 259-263.

Table of Contents Image: